Charge transfer and association of protons colliding with potassium from very low to intermediate energies

C. H. Liu,[1] Y. Z. Qu,[2,3,*] J. G. Wang,[1,3] Y. Li,[4] and R. J. Buenker[4]

[1]*Institute of Applied Physics and Computational Mathematics, Post Office Box 8009, Beijing 100088, People's Republic of China*

[2]*College of Material Sciences and Optoelectronic Technology, Graduate University of the Chinese Academy of Sciences, Post Office Box 4588, Beijing 100049, People's Republic of China*

[3]*Center of Theoretical Nuclear Physics, National Laboratory of Heavy Ion Collisions, Lanzhou 730000, People's Republic of China*

[4]*Fachbereich C-Mathematik und Naturwissenschaften, Bergische Universität Wuppertal, D-42097 Wuppertal, Germany*

(Received 29 September 2009; published 25 January 2010)

The nonradiative charge-transfer process for $H^+ + K(4s)$ collision is investigated using the quantum-mechanical molecular-orbital close-coupling method for collision energies from 1 eV to 10 keV. The radiative-decay and radiative charge transfer cross sections are calculated using the optical potential approach and the fully quantal method, respectively, for the energy range of 10^{-5}–10 eV. The radiative-association cross sections are obtained by subtracting the radiative charge-transfer part from total radiative-decay cross sections. The relevant molecular data are calculated from the multireference single- and double-excitation configuration interaction approach. The nonradiative charge transfer is the dominant mechanism at energies above 2 eV, whereas the radiative charge transfer becomes primary in the low-energy region of $E < 1.5$ eV. The present radiative-decay cross sections disagree with the calculations of Watanabe *et al.* [Phys. Rev. A **66**, 044701 (2002)]. The total charge-transfer rate coefficient is obtained in the temperature range of 1–20 000 K.

DOI: 10.1103/PhysRevA.81.012707 PACS number(s): 34.70.+e, 34.20.−b

I. INTRODUCTION

The charge transfer in collisions of protons with alkali-metal atoms affects the ionization balance in the atmospheres of planets, dwarf stars, and the interstellar medium [1–4]. Because of the near-resonant condition, these charge-exchange processes are known to possess large cross sections in a wide energy range and are also important in laboratory plasma environments [5–8]. At low temperature, such as in ultracold experiments, where collision energies are much smaller than 1 eV, nonradiative charge transfer can be important if favorable crossings occur in the potential curves of the initial and final diabatic states. In the absence of suitable crossings, the radiative charge transfer will often be more efficient through photon emission. In our previous work [9–11], several methods have been used to treat the radiative and nonradiative charge transfer, as well as the radiative-association processes for protons colliding with sodium. This experience has encouraged us to extend our investigations to the collision of protons with the heavier alkali-metal atom, potassium, to provide accurate data which can be useful in various applications. In the collisions of H^+ with the ground $4s$ state of K, the charge-exchange reaction may occur by nonradiative charge transfer,

$$H^+ + K(4s) \rightarrow H + K^+, \tag{1}$$

by radiative charge transfer,

$$H^+ + K(4s) \rightarrow H(1s) + K^+ + h\nu, \tag{2}$$

or by radiative association,

$$H^+ + K(4s) \rightarrow KH^+ + h\nu. \tag{3}$$

In the keV energy region, the nonradiative charge-transfer process (1) has been extensively investigated both experimentally and theoretically [12–18]. In this article, we study the process (1) in a wide energy range of 0.001–10 keV using a quantum-mechanical molecular-orbital close-coupling (QMOCC) method.

For energies below several eV, the radiative processes may become dominant over nonradiative charge transfer. The radiative decay process including both reactions (2) and (3) was investigated by Watanabe *et al.* [19] using the optical potential method. In our previous work [10], we pointed out errors in their calculations for protons colliding with sodium. In this work, we study the radiative-decay and radiative charge-transfer processes using the optical potential and the fully quantal methods, respectively. The radiative-decay results are compared with those of Watanabe *et al.* [19]. The radiative-association cross sections are obtained by taking differences between radiative-decay and radiative charge-transfer results. The rate coefficients including both radiative and nonradiative charge-transfer processes are presented. The molecular data needed are calculated using the multireference single- and double-excitation configuration interaction (MRD-CI) method.

II. THEORETICAL METHODS

A. Nonradiative charge transfer

The QMOCC method to describe nonradiative charge transfer in ion-atom collisions has been formulated in detail in the literature [20,21], and it is only briefly outlined in the present work. In the diabatic representation, the radial scattering amplitude describing the relative motion of the nuclei can be obtained by solving a coupled set of second-order differential equations written as

$$\left[\frac{d^2}{dR^2} - \frac{J(J+1)-\Lambda^2}{R^2} + 2\mu E\right] g_\gamma^J - 2\mu \sum_{\gamma'} U_{\gamma,\gamma'}(R) g_{\gamma'}^J = 0, \tag{4}$$

*yzqu@gucas.ac.cn

where μ is the reduced mass of the ion-atom pair, E is the relative collision energy in the center-of-mass frame, R is the coordinate of the relative nuclear motion, J is the total angular momentum quantum number, Λ is the projection of the total electronic angular momentum along the internuclear axis, and $U(R)$ is the diabatic potential matrix in which the off-diagonal elements are responsible for driving charge transfer in the diabatic representation [21,22], defined by

$$U(R) = W(R)[V(R) - P(R)]W^{-1}(R), \tag{5}$$

where $V(R)$ is the diagonal adiabatic potential matrix, $W(R)$ is the unitary transformation matrix that obeys the equation

$$\frac{dW(R)}{dR} + A^r(R)W(R) = 0, \tag{6}$$

and $P(R)$ is the rotational coupling matrix whose elements are given by [20,23]

$$P_{\alpha\beta} = \mp\frac{1}{\mu R^2}[(J \mp \Lambda_\alpha)(J \pm \Lambda_\alpha + 1)]^{1/2} A^\theta_{\alpha\beta}\delta(\Lambda_\alpha, \Lambda_\beta \pm 1). \tag{7}$$

The elements $A^r_{\alpha\beta}(R) = \langle\psi_\alpha|\frac{\partial}{\partial R}|\psi_\beta\rangle$ and $A^\theta_{\alpha\beta}(R) = \langle\psi_\alpha|iL_y|\psi_\beta\rangle$ are, respectively, the radial and rotational coupling matrix elements, with ψ_α and ψ_β being the adiabatic electronic eigenfunctions.

Equation (4) may be solved with the log-derivative method of Johnson [24]. The K matrix can be extracted from the scattering amplitude, and thus the scattering matrix S is given by

$$S_J = [I + iK_J]^{-1}[I - iK_J], \tag{8}$$

with I the identity matrix. Finally, the charge-transfer cross sections from channel α to channel β are expressed in terms of the scattering matrix elements,

$$\sigma_{\alpha\to\beta} = \frac{\pi}{k^2_\alpha}\sum_J (2J+1)|(S_J)_{\alpha\beta}|^2, \tag{9}$$

where k_α denotes the initial momentum.

B. Radiative charge transfer and radiative association

The radiative charge-transfer cross section in the fully quantum-mechanical approach [25–27] can be given by

$$\sigma = \int_{\omega_{\min}}^{\omega_{\max}} \frac{d\sigma}{d\omega}d\omega, \tag{10}$$

with

$$\frac{d\sigma}{d\omega} = \frac{8}{3}\left(\frac{\pi}{k_A}\right)^2 \frac{\omega^3}{c^3}\sum_J \left[J M^2_{J,J-1}(k_A, k_X) + (J+1)M^2_{J,J+1}(k_A, k_X)\right], \tag{11}$$

where ω is the angular frequency of the emitted photon and c is the speed of light. The subscripts A and X denote the upper and the lower states, respectively, and

$$M_{J,J'}(k_A, k_X) = \int_0^\infty dR f^A_J(k_A R)D(R)f^X_{J'}(k_X R), \tag{12}$$

where $D(R)$ is the transition dipole moment connecting the two electronic states and k_A and k_X are the entrance and exit momenta, respectively. The partial wave $f^i_J(k_i R)$ $(i = A, X)$ is the regular solution of the homogeneous radial equation

$$\left\{\frac{d^2}{dR^2} - \frac{J(J+1)}{R^2} - 2\mu[V_i(R) - V_i(\infty)] + k_i^2\right\} f^i_J(k_i R) = 0 \tag{13}$$

and normalized asymptotically according to

$$f^i_J(k_i R) = \sqrt{\frac{2\mu}{\pi k_i}}\sin\left(k_i R - \frac{J\pi}{2} + \delta^i_J\right), \tag{14}$$

with δ^i_J, $(i = A, X)$ the phase shifts.

On the other hand, the optical potential method [25,26,28] can be adopted to obtain the total cross sections for radiative decay, including both the radiative charge transfer and the radiative-association processes. The radiative-decay cross sections can be written as

$$\sigma(E) = \frac{\pi}{k^2_A}\sum_J^\infty (2J+1)[1 - \exp(-4\eta_J)], \tag{15}$$

and the phase shift η_J is given in the distorted-wave approximation as

$$\eta_J = \frac{\pi}{2}\int_0^\infty dR\left|f^A_J(k_A R)\right|^2 A(R), \tag{16}$$

where $A(R)$ is the transition probability for the radiative transition given by

$$A(R) = \frac{4}{3}D^2(R)\frac{|V_A(R) - V_X(R)|^3}{c^3}. \tag{17}$$

In order to extend the radiative-decay calculation to higher energy, replacing the summation in Eq. (15) and applying the Jeffrey-Wentzel-Kramers-Brillouin approximation, one obtains the expression for the semiclassical cross section

$$\sigma(E) = 2\pi\sqrt{\frac{2\mu}{E}}\int pdp\int_{R^{\rm ctp}_A}^\infty dR\frac{A(R)}{\sqrt{1 - V_A(R)/E - p^2/R^2}}, \tag{18}$$

where p is the impact parameter and $R^{\rm ctp}_A$ is the classical turning point in the incoming channel [25,29]. For relatively large energies ($E \gg V_A$), the double integral is nearly energy independent, and therefore $\sigma(E)$ varies as $1/E^{1/2}$ [26–28].

By subtracting the radiative charge-transfer part from the total radiative-decay cross sections, one obtains the radiative-association cross sections.

III. RESULTS AND DISCUSSIONS

A. Nonradiative charge transfer

In the present study, *ab initio* configuration-interaction (CI) calculations are carried out for potential curves of six Σ^+ electronic states in A_1 symmetry and two Π states in B_1 symmetry of the KH^+ molecule using the MRD-CI package [30,31]. In the calculation of hydrogen, the correlation-consistent, polarization valence, quadruple-ζ (cc-pVQZ) basis set [32] is used. In addition to the above basis set, $(2s3p)$ diffuse functions are added. The final contracted basis set for the hydrogen atom is $(8s, 6p, 2d, 1f)/[6s, 6p, 2d, 1f]$. For the potassium atom, an effective core potential (ECP) [33] is employed to describe the

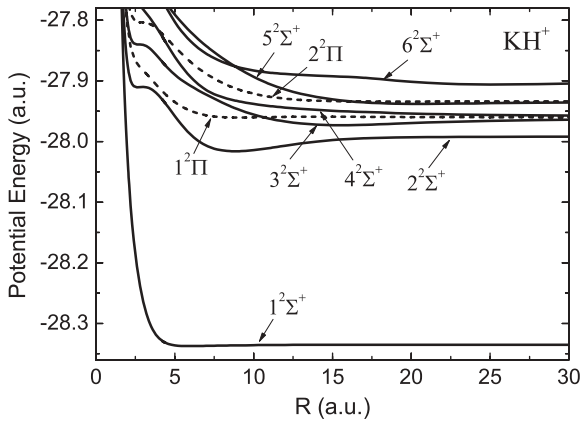

FIG. 1. Adiabatic potential curves for $(KH)^+$. The solid and dashed lines refer to the Σ^+ and Π channels, respectively.

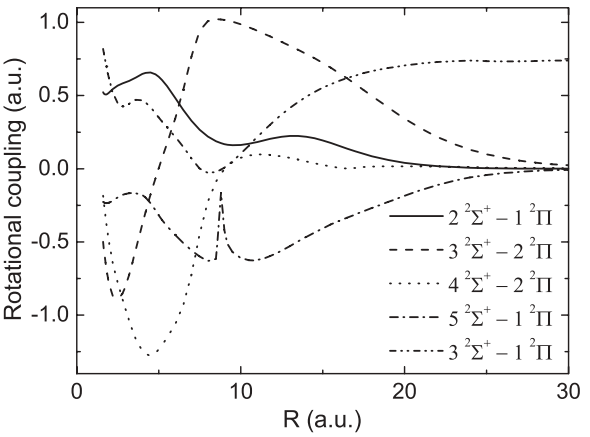

FIG. 3. Rotational coupling matrix elements for KH^+.

ten core electrons, whereby only the remaining nine valence electrons need to be considered explicitly in the *ab initio* self-consistent-field (SCF) and CI calculations. The ECP-adapted $(5s4p)$ Gaussian basis set [33] without contraction is employed for the $3s$, $3p$, and $4s$ subshells. A diffuse $(1s\ 2p\ 4d\ 1f)$ basis is employed for describing its Rydberg states. A threshold of 10^{-10} Hartree is used to select the configurations [30] of which the electronic wave functions are composed. The errors in our calculated energies for the considered electronic states are no more than 0.07 eV in the asymptotic region. The obtained electronic wave functions are then employed to calculate radial and rotational couplings by using finite differentiation and analytical approaches, respectively [34].

The adiabatic potentials are displayed in Fig. 1, in which $1^2\sum^+$, $2^2\sum^+$, $3^2\sum^+$, $4^2\sum^+$, $5^2\sum^+$, $6^2\sum^+$, $1^2\Pi$, and $2^2\Pi$ correspond to $K^+ + H(1s)$, $K(4s) + H^+$, $K^+ + H(2p\sigma^+)$, $K^+ + H(2p\sigma^-)$, $K(4p\sigma) + H^+$, $K(5s) + H^+$, $K^+ + H(2p\pi)$, and $K(4p\pi) + H^+$ states in the asymptotic region, respectively. The $2^2\sum^+$ state represents the initial channel for our considered processes. The shallow wells, appearing at $R \approx 3$ a.u. in the potential curves except for the $1^2\sum^+$ state appear to be caused by the excitation of the inner $3p$ shell electrons of the K atom. These wells did not appear in other theoretical works [12,35,36], in which the KH^+ molecule was treated as an effective one-electron system and the inner $3p$ shell electrons were not excited. Because this difference only exists at very small internuclear separation in a narrow range, it may have no apparent impact on the scattering cross sections, especially for the low-energy results.

In Figs. 2 and 3, we show some important radial and rotational couplings, respectively. It is evident that the positions of the peaks in radial couplings are consistent with the avoided crossings of the adiabatic potentials. The main gateway to the charge exchange will be the $2^2\sum^+$–$3^2\sum^+$ and $2^2\sum^+$–$1^2\prod$ couplings because of the very close encounters in the associated potential curves. In comparison to the NaH^+ case [9], the shapes of the couplings are similar, but the regions of the peaks for KH^+ shift to comparatively larger internuclear separations. This is because the scale of the K (K^+) atom (ion) is larger than that of the Na (Na^+) atom (ion) and will result in the larger cross sections in the low-energy region. It should be noted that in our calculations of radial couplings, the origin of electronic coordinates is placed at the mass center of the collision system. Furthermore, at higher energies in a semiclassical, impact-parameter approach, it is possible to include electron translation factors (ETFs) [37] (such as of the plane-wave type), which leads to matrix elements that have the correct boundary conditions and are independent of the choice of origin and are simple in the zero-velocity limit. But in this article, ETFs are not included in our description of the collision. Since the influence of ETFs is expected to be important when the incident energy $E > 1$ keV/u [38,39], the validity of our calculations is restricted to the low-impact-energy region (typically $E < 5$ keV/u [9]).

Using the potentials and couplings described above, we calculated the nonradiative charge-transfer cross sections using the QMOCC method for $H^+ + K(4s)$ collision in the energy range of 0.001–10 keV. Since Saha and Kumar [35] have tested

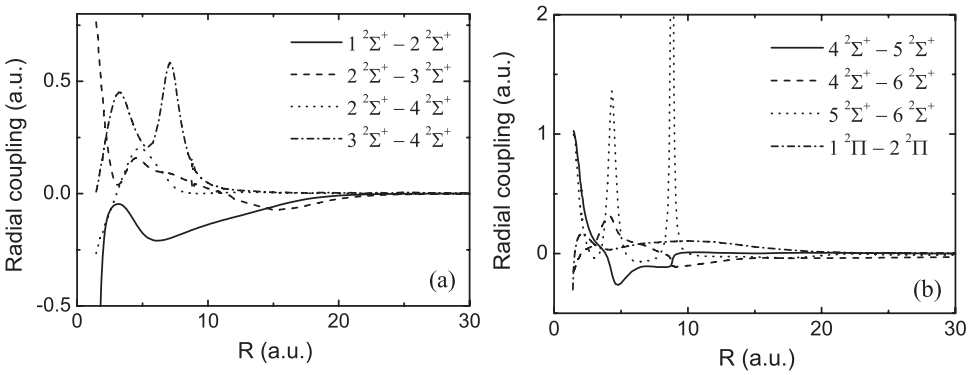

FIG. 2. Radial coupling matrix elements for KH^+.

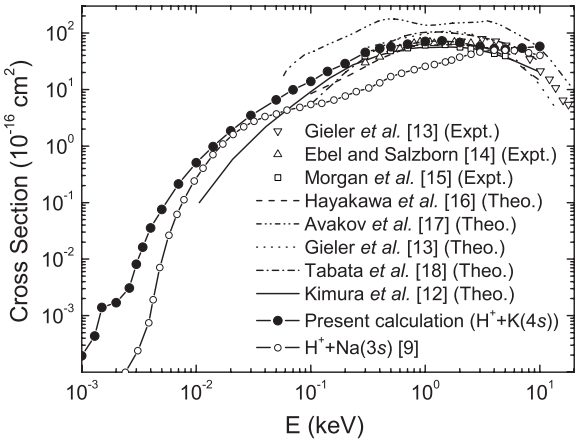

FIG. 4. The total nonradiative charge-transfer cross sections of the present calculation and other results for $H^+ + K(4s)$ collisions, and comparison with the results for $H^+ + Na(3s)$ collisions. Theoretical results: present QMOCC calculation (solid line with filled circles), Kimura *et al.* [12] (solid line), Gieler *et al.* [13] (dotted line), Hayakawa *et al.* [16] (dashed line), Avakov *et al.* [17] (dash-dot-dotted line), Tabata *et al.* [18] (dash-dotted line); experimental results: Gieler *et al.* [13] (open downward triangle), Ebel and Salzborn [14] (open up triangle), Morgan *et al.* [15] (open squares). The open circles represent the results of $H^+ + Na(3s)$ collisions [9].

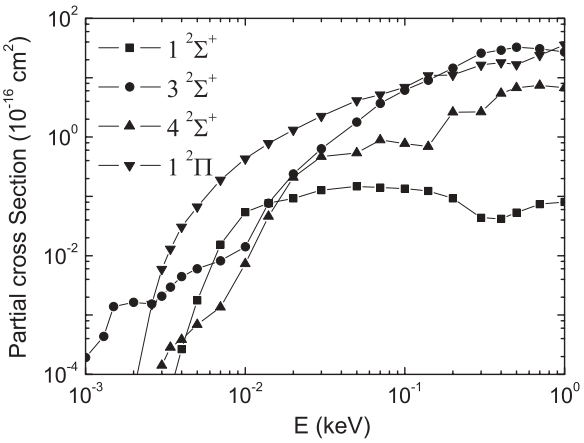

FIG. 5. State-selected nonradiative charge-transfer cross sections for $H^+ + K(4s)$ collision.

in their ten-state calculations for the $H^+ + K(4p)$ collision, our eight-state results should be a good approximation for the $H^+ + K(4s)$ collision, especially at low energies. The total nonradiative charge-transfer cross sections are displayed in Fig. 4, and compared with other experimental and theoretical results. In the keV energy region, a number of experimental measurements [13–15] and theoretical calculations [12,13,16–18] have been performed. Our QMOCC results are in good agreement with these results in the overlapping energy region of 0.1–5 keV. There is no experimental work in the low-energy region for $E < 100$ eV, and only Kimura *et al.* [12] report theoretical results obtained by semiclassical MOCC methods. Our results are larger than theirs at energies less than 100 eV. This is similar to what was obtained in previous calculations on $H^+ + Na(3s)$ [9,12]. Kimura *et al.* [12] mentioned that in the internuclear separation $R \approx 18$ a.u. there is a strong radial coupling between the $4^2\sum^+$ and $5^2\sum^+$ states, which resulted in a loss of about two-thirds of the charge-transfer flux in the low-energy region. However, in our MRD-CI calculations, we do not find this apparent coupling at $R \approx 18$ a.u., and consistent with this finding, no avoided crossing is found in either their [12] or our potential curves. In fact, their semiclassical treatment for the scattering calculation and the effective one-electron approximation for the KH^+ molecular structure calculation may be responsible for this discrepancy. At energies larger than about 5 keV/u, our QMOCC cross sections increase with increasing collision energy, whereas the other theoretical and experimental results decrease gradually. This is because we have not included ETFs, which may be important in this relatively high-energy region.

The cross sections for $H^+ + Na(3s)$ charge transfer [9] are also presented in Fig. 4 for comparison. The maximum cross section for $H^+ + K(4s)$ collisions is larger than that for the $H^+ + Na(3s)$ collisions and occurs at a lower energy. This is because the energy defect for $H^+ + K(4s)$ collisions between $2^2\sum^+$ and $3^2\sum^+$ (0.94 eV) is smaller than $H^+ + Na(3s)$ (1.74 eV), and the ionization energy of K(4*s*) (4.34 eV) is smaller than that of Na(3*s*) (5.14 eV) [40]. The cross sections for $H^+ + K(4s)$ collisions are larger than those for $H^+ + Na(3s)$ in the low-energy region. This is in agreement with the results for the aforementioned comparisons for nonadiabatic couplings.

The state-selected cross sections are shown in Fig. 5. The calculation shows that the partial cross sections to the $3^2\sum^+$ channel dominante at energies below 2.5 eV, and the $1^2\Pi$ state will become the most important charge-transfer final state in the intermediate-energy region. The charge-transfer processes to these two channels compete with each other at energies above 100 eV. This is consistent with the energy gaps between $2^2\sum^+$ and other potential curves (see Fig. 1), as well as with the magnitude of the relevant couplings.

In the higher-energy region ($E > 100$ eV), the charge-transfer processes are mainly induced by the couplings at small internuclear separations, where the potential curves $2^2\sum^+$, $3^2\sum^+$, and $1^2\Pi$ come very close to each other. All of the couplings among these three states will influence the charge-transfer results, and then the electron occupation in these states indicates close competition between these processes.

As the the energy decreases, the efficient internuclear separation range moves to a larger region and the energy gap between the $2^2\sum^+$ and the $3^2\sum^+$ states increases. The potential curves of the $2^2\sum^+$ and $1^2\Pi$ states come closer and are almost degenerate at $R \approx 18$ a.u. The most efficient mechanism for populating the excited states will be via the rotational coupling between the $2^2\sum^+$ and the $1^2\Pi$ states at $R \approx 18$ a.u.

As the collision energies decrease further and go below 2.5 eV, the classical turning point for each partial wave will move to larger R, where the energy gap between the $2^2\sum^+$ and the $1^2\Pi$ curves is larger (see Fig. 1), thus making rotational coupling relatively inefficient, with the result that the partial charge-transfer cross section to $1^2\Pi$ drops rapidly. For the radial coupling between the $2^2\sum^+$ and the $3^2\sum^+$ states, the avoided crossing is around 15 a.u., but the energy gap is relatively large compared to that of the $1^2\Pi$ channel at small

R, and hence, this is not an efficient mechanism for making a direct transition for energies larger than 2.5 eV. However, at energies below 2.5 eV, this avoided crossing around 15 a.u. drives the charge-transfer processes and the cross sections to the $3^2\sum^+$ channel become dominant.

B. Radiative-decay, radiative charge-transfer, and radiative-association processes

In this work, for radiative processes, the upper A and the lower X states in Eqs. (10)–(18) correspond to the $2^2\sum^+$ and the $1^2\sum^+$ states, respectively. Because the $2^2\sum^+$ state is the initial channel, one only need consider it and the lower $1^2\sum^+$ states. The dipole matrix element between $1^2\sum^+$ and $2^2\sum^+$ is shown in Fig. 6, and our results are in good agreement with those of Watanabe *et al.* [19] and Magnier [36], especially at relatively large internuclear separation, where it provides the main contribution for low-energy processes.

Using Eq. (17), we calculated the transition probability $A(R)$, as shown in Fig. 7. It increases as the internuclear distance increases, reaching a maximum at $R \approx 5.5$ a.u. and then decreases gradually thereafter. Our calculated $A(R)$ is similar in shape to that of Watanabe *et al.* [19]. But the unit of $A(R)$ in Ref. [19], shown as 10^{-8} s^{-1}, is apparently an error, so that our $A(R)$ cannot be compared to theirs directly. For comparison, the transition probability for $H^+ + Na(3s)$ collisions [10] is also given in Fig. 7. Similarly as in the case of radial or rotational couplings, the peak of $A(R)$ for $H^+ + K(4s)$ appears at a larger internuclear separation, and then the magnitude of $A(R)$ for $H^+ + K(4s)$ is larger than that of $H^+ + Na(3s)$ at $R > 5$ a.u.

Beyond $R = 30$ a.u., the potential of the $2^2\sum^+$ state can be described by the long-range form

$$V_L(R) = -\frac{1}{2}\left[\frac{C_4}{R^4} + \frac{C_6}{R^6} + \frac{C_8}{R^8}\right], \tag{19}$$

where C_4, C_6, and C_8 are the dipole, quadrupole, and octupole polarizabilities of the K(4s) atom, respectively. For convenience of comparison, they are chosen to be the same as those used in Ref. [19]. For the ground state $1^2\sum^+$, the form of the long-range potential is $V_L(R) = -(1/2)(\alpha_d/R^4)$,

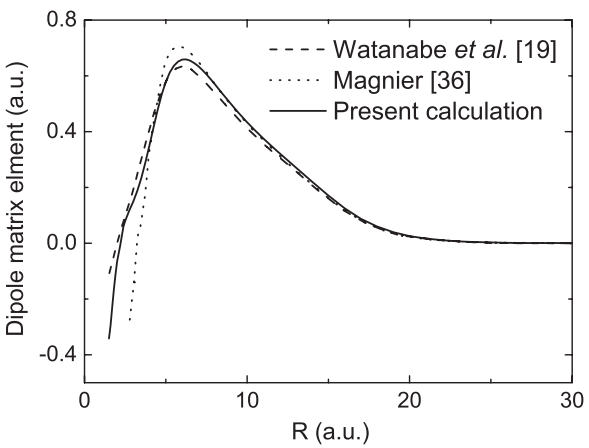

FIG. 6. Dipole matrix element between $1^2\sum^+$ and $2^2\sum^+$ states. Present calculation (solid line), Watanabe *et al.* [19] (dashed line), Magnier [36] (dotted line).

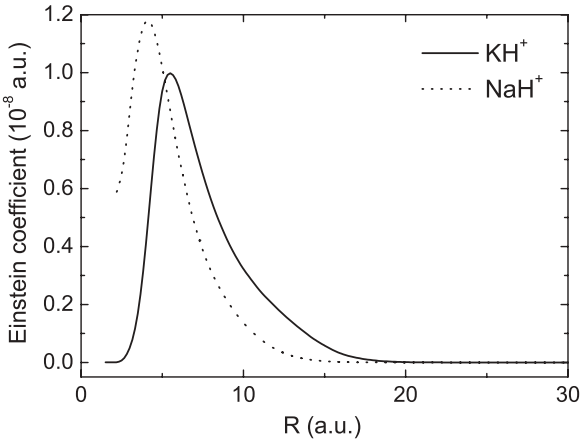

FIG. 7. Transition probability $A(R)$ between the $1^2\sum^+$ and the $2^2\sum^+$ states for $H^+ + K(4s)$ and $H^+ + Na(3s)$ collisions [10].

where α_d is the dipole polarizability of the H(1s) atom. The long-range asymptotic behavior of the dipole matrix element is fitted to the form d_0/R^n.

Using the optical potential method, we have calculated the radiative-decay cross sections for energies from 10^{-5} to 10 eV, as shown in Fig. 8. The cross sections decrease as the collision energy increases. Rich resonance structures appear in the energy range of 10^{-5}–0.3 eV. These resonances are attributed to the presence of quasibound or virtual rotational-vibrational levels in the entrance channel, and may give rise to an enhancement of the rate coefficients [26,28]. In order to extend the treatment to higher energy, we also performed a semiclassical calculation using Eq. (18) at the higher-energy region of 1–100 eV, as shown in Fig. 8. In the overlapping 1–10 eV energy range, the optical-potential cross sections are in agreement with the semiclassical results.

In Fig. 8, our radiative-decay cross sections are compared with the results of Watanabe *et al.* [19]. Perhaps because of the fewer calculated energy points, they did not find the rich resonance structures. In addition, for collision energy

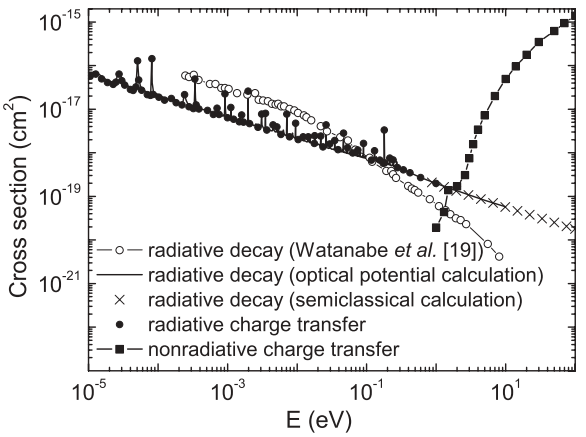

FIG. 8. Radiative-decay and radiative charge-transfer cross sections for $H^+ + K(4s)$ collisions. Radiative-decay results: the optical potential method (solid line), the semiclassical method (crosses), Watanabe *et al.* [19] (solid line with open circles). Radiative charge-transfer results (filled circles). Nonradiative charge-transfer results (solid line with filled squares).

$E < 10^{-2}$ eV, their calculated cross sections are about four times larger than ours except at the positions of resonances. Our cross sections have an energy dependence of $1/E^{1/2}$, which is consistent with the Langevin cross-section formula for a polarization potential. But the cross sections of Watanabe *et al.* [19] have the $1/E$ dependence at energies above 10^{-2} eV. As in our previous work [10], we re-examined the optical potential calculations using the code of Ref. [41], the same as that used by Watanabe *et al.* [19]. We arrive at the same conclusion as in our previous article, that is, the probable imprecision in the calculation of Watanabe *et al.* [19] results in an incorrect energy dependence of the cross sections, and the discrepancy in the magnitude of the cross sections probably comes from the difference in transition probability $A(R)$.

The radiative charge-transfer cross sections calculated from the fully quantum-mechanical approach are also shown in Fig. 8 by filled circles. Since the lower $1^2\sum^+$ state of the present system only has a very shallow well (~0.056 eV) at short range, the radiative charge transfer is responsible for most of the radiative-decay process [10,28]. For comparison, the nonradiative charge-transfer results are displayed in the same figure. Below 1.5 eV, the radiative charge-transfer process is the dominant charge-transfer mechanism. As the collision energy increases, the nonradiative charge-transfer cross sections show a sharp increase and become dominant over the radiative results at energies above 2 eV.

The radiative-association cross sections, which are obtained by subtracting the radiative charge-transfer part from the radiative-decay cross sections, are displayed in Fig. 9 and compared with the radiative-decay results, as well as with the corresponding results for the $H^+ + Na(3s)$ collisions [10,11]. The radiative-association cross sections are about one order of magnitude smaller than the radiative-decay results at energies from 0.01 to 0.3 meV. As the collision energies increase, the difference between the radiative-decay and the charge-transfer cross sections decreases (see Fig. 8). The radiative-association cross sections decrease more rapidly than the radiative-decay results. This is because the interaction time for emitting the radiation is reduced [42] as the collision energy is increased. Since the radiative-association cross sections are obtained as differences between the radiative-decay and the charge-transfer results in our calculation, the accuracy is not sufficient in the energy region of $E > 1$ meV, and the radiative-association cross section become increasingly less smooth, especially at the position of resonances.

The comparison with the results for $H^+ + Na(3s)$ collisions shows that the radiative-decay cross sections for $H^+ + K(4s)$ collisions are about two times larger than those of $H^+ + Na(3s)$, but the radiative-association results of $H^+ + K(4s)$ differ very little from those of $H^+ + Na(3s)$ at energies less than 0.3 meV, even becoming smaller than those of $H^+ + Na(3s)$ collisions at larger energies. The difference in radiative-decay cross sections is caused primarily by the differences in transition probability $A(R)$. As mentioned earlier in this article, the results for the low-energy region rely on the molecular data at large internuclear separation. For the $H^+ + K(4s)$ collision, the larger $A(R)$ at $R > 5$ a.u. results in greater radiative-decay cross sections. But the radiative association depends on not only the dipole matrix element, but also the shape of the potential well in the final state. Because the well of the lower $1^2\sum^+$ state for KH^+ (0.056 eV) is shallower than that of NaH^+ (0.125 eV) [10], the radiative-association cross sections for $H^+ + K(4s)$ do not appear to be larger than those of $H^+ + Na(3s)$. Because the effective angular momentum quantum numbers increase with collision energy, for the $H^+ + K(4s)$ collisions, the shallower well in the effective potentials $V_j^{\text{eff}}(R) = V(R) + (J+1)/2\mu R^2$ of the $1^2\sum^+$ state will disappear at a relative small value of J, causing the radiative-association cross sections to decrease more rapidly than for the $H^+ + Na(3s)$ collisions.

In many application fields, such as in astrophysics, the rate coefficients are needed. In this work, the rate coefficients for temperatures between 1 and 20 000 K are obtained by averaging the radiative and nonradiative charge-transfer cross sections over a Maxwellian velocity distribution. The results are displayed in Fig. 10 and compared to those of Watanabe

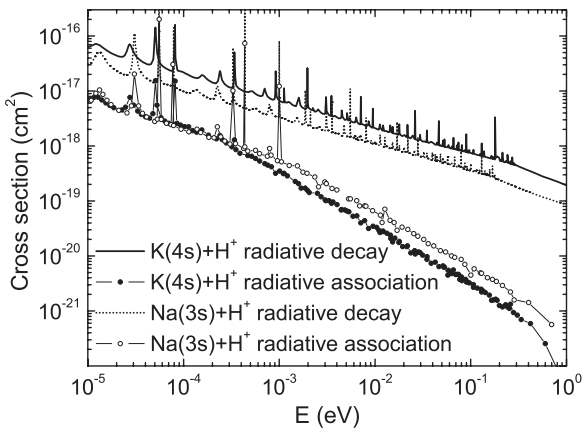

FIG. 9. Comparison of the radiative-decay and radiative-association cross sections for both $H^+ + K(4s)$ and $H^+ + Na(3s)$ collisions [10,11]. $H^+ + K(4s)$: radiative decay (solid line), radiative association (solid line with filled circles); $H^+ + Na(3s)$: radiative decay (dotted line), radiative association (solid line with open circles).

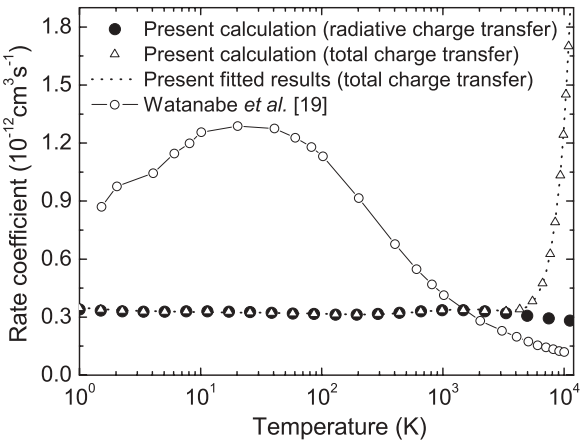

FIG. 10. Raditive and nonradiative charge-transfer rate coefficients as a function of temperature. Only the radiative charge-transfer process is included: present calculation (filled circles), Watanabe *et al.* [19] (solid line with open circles). Both radiative and nonradiative charge-transfer processes are included: present calculation (open triangles), present fitted results (dotted lines).

TABLE I. Rate coefficients for radiative and nonradiative charge-transfer processes in $H^+ + K(4s)$ collisions. Units for a_i and c_i are 10^{-12} cm^3 s^{-1} and Kelvin, respectively.

T (K)	$\alpha(T)$ (10^{-12} cm^3 s^{-1})
1.0	0.347
2.0	0.334
4.0	0.328
6.0	0.328
8.0	0.329
10	0.330
20	0.326
40	0.321
60	0.318
80	0.316
100	0.315
200	0.314
400	0.321
600	0.328
800	0.333
1000	0.336
2000	0.336
4000	0.315
6000	0.414
8000	0.684
10 000	1.283
20 000	12.78
a_1	0.0494
b_1	−0.164
c_1	178.8
a_2	0.533
b_2	0.156
c_2	9737
a_3	2.097
b_3	4.47
c_3	15415

et al. [19]. In the latter study, the unit of rate coefficients (10^{12} cm^3 s^{-1}) given is apparently a typographical error, and we have modified it in Fig. 10. For a specific temperature, the rate coefficients mainly come from energies lower than five times of the energies corresponding to that temperature. Our rate coefficient approaches a constant value of approximately 3.3×10^{-13} cm^3 s^{-1} at $T < 4000$ K. This is because in this temperature region, the rate coefficients are mainly due to the radiative charge-transfer cross section, which behaves as $1/E^{1/2}$. The total charge-transfer rate coefficients increase sharply in the temperature region of $T > 5000$ K because the contribution from the nonradiative charge-transfer process becomes dominant at energies above 2 eV. The radiative charge-transfer rate coefficients of Watanabe *et al.* [19] have a very different temperature dependence than the present calculation. Their results vary smoothly at $T < 100$ K and then decrease rapidly for $T > 100$ K. Our rate coefficients are a few times smaller than those of Watanabe *et al.* at $T < 1000$ K and become larger than theirs at $T > 1500$ K. The distinctions in the computed rate coefficients are consistent with the discrepancy noted in the associated cross sections.

For convenience in future applications, the rate coefficients, including both the radiative and the nonradiative charge-transfer processes are given in Table I at temperatures between 1 and 20 000 K. We also fitted the rate coefficients to the form

$$\alpha(T) = \sum_i a_i \left(\frac{T}{10000}\right)^{b_i} \exp\left(-\frac{T}{c_i}\right). \qquad (20)$$

The fitting parameters are provided at the end of Table I. Units for a_i and c_i are 10^{-12} cm^3 s^{-1} and Kelvin, respectively. The fitting is reliable to within 2% over the temperature range of 1–20 000 K. The fitted data are also plotted in Fig. 10.

IV. CONCLUSION

We have calculated the total and state-selective nonradiative charge-transfer cross sections for protons colliding with K(4*s*) atoms in a wide energy range of 0.001–10 keV using the QMOCC method. The radiative-decay process is investigated using the optical-potential and semiclassical methods for collision energy ranges of 10^{-5}–10 eV and 0.01–100 eV, respectively. The radiative charge-transfer cross sections are calculated by the fully quantum method. We obtain the radiative-association results by subtracting the radiative charge-transfer part from the radiative-decay cross sections. The calculations utilize *ab initio* molecular data obtained from the MRD-CI approach. The nonradiative charge transfer is the dominant mechanism at energies above 2 eV, and the radiative charge transfer becomes the primary mechanism for energies below 1.5 eV. Our radiative-decay results generally disagree with the calculations of Watanabe *et al.* [19]. The discrepancy in the magnitude of the radiative-decay cross sections appears to be caused by differences of transition probability, and the distinction in the energy dependence of the cross sections are probably due to the inadequate precision in the calculation of Watanabe *et al.* [19]. The total radiative and nonradiative charge-transfer rate coefficient is also obtained for temperatures between 1 and 20 000 K, which also differs dramatically from the results of Watanabe *et al.* [19].

ACKNOWLEDGMENTS

This work was supported in part by NSF of China under Grants No. 10774186 and No. 10676014, by NASF under Grant No. 10876043, and the National Key Laboratory of Computational Physics Foundation under Grant No. 9140C6904030808.

[1] R. E. Johnson, Icarus **143**, 429 (2000).
[2] G. E. Langer, C. F. Prosser, and C. Sneden, Astron. J. **100**, 216 (1990).
[3] A. Burrows, W. B. Hubbard, J. I. Lunine, and J. Liebert, Rev. Mod. Phys. **73**, 719 (2001).
[4] D. Sudarsky, A. Burrows, and P. Pinto, Astrophys. J. **538**, 885 (2000).
[5] R. K. Janev, in *Atomic and Molecular Processes in Fusion Edge Plasma* (Plenum, New York, 1995).
[6] R. E. Olson, R. P. Saxon, and B. Liu, J. Phys. B **13**, 297 (1980).

[7] J. K. Berkowitz and J. C. Zorn, Phys. Rev. A **29**, 611 (1984).
[8] A. Cornet *et al.*, J. Phys. B **22**, L647 (1989).
[9] C. H. Liu, Y. Z. Qu, L. Liu, J. G. Wang, Y. Li, H.-P. Liebermann, P. Funke, and R. J. Buenker, Phys. Rev. A **78**, 024703 (2008).
[10] C. H. Liu, Y. Z. Qu, Y. Zhou, J. G. Wang, Y. Li, and R. J. Buenker, Phys. Rev. A **79**, 042706 (2009).
[11] C. H. Liu, Y. Z. Qu, J. G. Wang, Y. Li, and R. J. Buenker, Phys. Lett. **A373**, 3761 (2009).
[12] M. Kimura, R. E. Olson, and J. Pascale, Phys. Rev. A **26**, 3113 (1982).
[13] M. Gieler, P. Ziegelwanger, F. Aumayr, H. Winter, and W. Fritsch, J. Phys. B **24**, 647 (1991).
[14] F. Ebel and E. Salzborn, J. Phys. B **20**, 4531 (1987).
[15] T. J. Morgan, R. E. Olson, A. S. Schlachter, and J. W. Gallagher, J. Phys. Chem. Ref. Data **14**, 971 (1985).
[16] S. Hayakawa, K. Kadomura, M. Kimura, and C. M. Dutta, Phys. Rev. A **70**, 022708 (2004).
[17] G. V. Avakov, L. D. Blokhintsev, A. S. Kadyrov, and A. M. Mukhamedzhanov, J. Phys. B **25**, 213 (1992).
[18] T. Tabata *et al.*, Nucl. Instrum. Methods Phys. Res. B **31**, 375 (1988).
[19] A. Watanabe, C. M. Dutta, P. Nordlander, M. Kimura, and A. Dalgarno, Phys. Rev. A **66**, 044701 (2002).
[20] B. H. Bransden and M. R. C. McDowell, in *Charge Exchange and the Theory of Ion-Atom Collisions* (Clarendon, Oxford, 1992).
[21] B. Zygelman, D. L. Cooper, M. J. Ford, A. Dalgarno, J. Gerratt, and M. Raimondi, Phys. Rev. A **46**, 3846 (1992).
[22] T. G. Heil, S. E. Butler, and A. Dalgarno, Phys. Rev. A **23**, 1100 (1981).
[23] A. R. Turner, D. L. Cooper, J. G. Wang, and P. C. Stancil, Phys. Rev. A **68**, 012704 (2003).
[24] B. R. Johnson, J. Comput. Phys. **13**, 445 (1973).
[25] B. Zygelman and A. Dalgarno, Phys. Rev. A **38**, 1877 (1988).
[26] P. C. Stancil and B. Zygelman, Astrophys. J. **472**, 102 (1996).
[27] L. B. Zhao, P. C. Stancil, J. P. Gu, H.-P. Liebermann, Y. Li, P. Funke, R. J. Buenker, B. Zygelman, M. Kimura, and A. Dalgarno, Astrophys. J. **615**, 1063 (2004).
[28] L. B. Zhao, J. G. Wang, P. C. Stancil, J. P. Gu, H.-P. Liebermann, R. J. Buenker, and M. Kimura, J. Phys. B **39**, 5151 (2006).
[29] D. R. Bates, Mon. Not. R. Astron. Soc. **111**, 303 (1951).
[30] R. J. Buenker and S. D. Peyerimhoff, Theor. Chim. Acta **35**, 33 (1974); **39**, 217 (1975); R. J. Buenker, Int. J. Quantum Chem. **29**, 435 (1986).
[31] R. J. Buenker, in *Proceedings of the Workshop on Quantum Chemistry and Molecular Physics*, edited by P. G. Burton (Wollongong University Press, Wollongong, Australia, 1980); in *Study in Physical and Theoretical Chemistry, Current Aspects of Quantum Chemistry*, edited by R. Carbo (Elsvier, Amsterdam, 1981), Vol. 21, p. 17; R. J. Buenker and R. A. Phillips, J. Mol. Struct.: THEOCHEM: **123**, 291 (1985); S. Krebs and R. J. Buenker, J. Chem. Phys. **103**, 5613 (1995).
[32] T. H. Dunning Jr., J. Chem. Phys. **90**, 1007 (1989).
[33] M. M. Hurley, L. F. Pacios, P. A. Christiansen, R. B. Ross, and W. C. Ermler, J. Chem. Phys. **84**, 6840 (1986).
[34] G. Hirsch, P. J. Bruna, R. J. Buenker, and S. D. Peyerimhoff, Chem. Phys. **45**, 335 (1980).
[35] B. C. Saha and A. Kumar, Phys. Rev. A **64**, 012721 (2001).
[36] S. Magnier, Chem. Phys. **326**, 375 (2006).
[37] M. Kimura and N. F. Lane, Adv. At. Mol. Opt. Phys. **26**, 79 (1990).
[38] J. G. Wang, P. C. Stancil, A. R. Turner, and D. L. Cooper, Phys. Rev. A **67**, 012710 (2003).
[39] L. F. Errea, C. Harel, H. Jouin, L. Méndez, B. Pons, and A. Riera, J. Phys. B **27**, 3603 (1994).
[40] B. L. Donnally, T. Clapp, W. Sawyer, and M. Schultz, Phys. Rev. Lett. **12**, 502 (1964).
[41] A. C. Allison, Comput. Phys. Commun. **3**, 173 (1972).
[42] F. A. Gianturco and P. Gori Giorgi, Astrophys. J. **479**, 560 (1997).